

Discretisation of an Oldroyd-B viscoelastic fluid flow using a Lie derivative formulation

Ben S. Ashby and Tristan Pryer

*Institute for Mathematical Innovation,
University of Bath, Bath, UK.*

*Department of Mathematical Sciences,
University of Bath, Bath, UK.*

Abstract

In this article we present a numerical method for the Stokes flow of an Oldroyd-B fluid. The viscoelastic stress evolves according to a constitutive law formulated in terms of the upper convected time derivative. A finite difference method is used to discretise along fluid trajectories to approximate the advection and deformation terms of the upper convected derivative in a simple, cheap and cohesive manner, as well as ensuring that the discrete conformation tensor is positive definite. A full implementation with coupling to the fluid flow is presented, along with detailed discussion of the issues that arise with such schemes. We demonstrate the performance of this method with detailed numerical experiments in a lid-driven cavity setup. Numerical results are benchmarked against published data, and the method is shown to perform well in this challenging case.

1 Introduction

Viscoelastic fluids produce a number of phenomena distinct from the familiar behaviour of Newtonian fluids. A broad class of such fluids is that of polymer solutions, for which these phenomena are the result of long chain molecules in the fluid that are large enough to have a meaningful effect on the fluid flow. Such fluids are found in industry in the form of molten plastics or machine lubricants, as well as several biological fluids such as blood. Polymeric fluids are modelled by augmenting the usual fluid flow equations for conservation of mass and momentum with a constitutive law for the polymeric stress, which results in a system of either partial differential or integro-differential equations. This article will focus on the former, with the constitutive law given by a hyperbolic partial differential equation (PDE).

In Newtonian fluid dynamics, the *Reynolds number* indicates the relative scaling of inertial terms to viscous terms in the Navier-Stokes equations, and can be used to predict flow behaviour and transition between different regimes such as laminar and turbulent flow. In viscoelastic flows, there are two dimensionless groups which are used to predict flow behaviour, the *Weissenberg number*, Wi and the *Deborah number*,

De. The Weissenberg number quantifies the effect of nonlinearities that arise due to non-Newtonian normal stress differences [11, 33]. The Deborah number has been interpreted as the ratio of the magnitudes of elastic and viscous forces [4]. In the limit as $De \rightarrow 0$, Newtonian flow behaviour is recovered. Experimental results for dilute polymer solutions reported in [32] suggest that a transition to turbulent flow behaviour may occur when elastic effects become dominant over viscous, an effect known as elastic instability, even for small Reynolds number. In complex flow geometries and time-dependent flows, it may be difficult to define these dimensionless groups appropriately, and indeed one may be more relevant than the other. However, in keeping with much of the literature on numerical methods for non-Newtonian flows, we will mainly consider the Weissenberg number Wi , defined as

$$Wi := \frac{\lambda U}{L},$$

where λ is the relaxation time and U and L are characteristic velocity and length scales of the problem.

Numerical methods posed for the solution of viscoelastic fluid problems, especially using the Oldroyd-B model, have been observed to suffer from the so-called high Weissenberg number problem, where numerical simulations fail to converge at moderate values of the Weissenberg number. There are several potential causes of the high Weissenberg number problem such as the fact that many viscoelastic fluid flow problems exhibit strong, spatially exponential layers which require fine mesh resolution to adequately resolve. In [34], the authors observe a relationship between the Weissenberg number and the principle eigenvalue, determined by numerical simulation and curve fitting. They find that this maximum value increases exponentially with respect to Wi . It is therefore a significant computational cost to resolve this layer for larger Weissenberg number. It has also been suggested that the Oldroyd-B model itself is insufficient to properly describe viscoelastic behaviour. Indeed, extensional viscosity of the Oldroyd-B model blows up at a finite strain rate [21]. Despite this, the Oldroyd-B model remains a popular test case for numerical modelling. This point is discussed in greater detail in §2.

It is also well known that for the Oldroyd-B model, if the initial data for the conformation tensor is positive definite, then the conformation tensor remains so for all time [13, 40]. Loss of positive definiteness at the discrete level is often a precursor to numerical blowup, and indeed it was shown in [42] that the Upper-convected Maxwell model (which is the model that results if the solvent contribution is neglected in the Oldroyd-B model) becomes ill-posed. It therefore appears that designing schemes which preserve the positive definiteness of the discrete conformation tensor is important not only to maintain the physical structures of the model, but also crucial for numerical stability.

These phenomena motivated what seems to be the dominant method for solving viscoelastic constitutive laws in differential form: the log-conformation representation, introduced in [15]. In this approach, a differential equation is derived for the tensor logarithm of the (positive definite) conformation tensor, thus guaranteeing that the numerical approximation to the conformation tensor will remain positive definite. It is argued that this method is more appropriate for resolving exponential spatial layers, and indeed has provided numerical simulations with relatively large Weissenberg numbers [16, 23] which are stable, though questions of accuracy remain. It is however suggested by the results of [45] that careful application of the method is required to preserve physical characteristics of the model. In particular, they report reduced turbulent drag reduction. In addition, solving for the logarithm of the conformation tensor introduces additional nonlinearities into the numerical model that are not present in the physical model, increasing computational expense. Other schemes which preserve positivity have been derived using for example the square root of

the conformation tensor [28] and the use of the hyperbolic tangent transformation [24].

Schemes based on a Lie derivative formulation offer a potential solution to the issues described above. While characteristic schemes are motivated by the idea of discretising the material derivative as a single object after expressing it as a rate along fluid trajectories, the upper-convected derivative is similarly expressible as a rate along fluid paths, this time including information on deformation of the moving fluid. Indeed, when expressed in a convected coordinate system, the Oldroyd-B constitutive law is a tensor-valued ordinary differential equation. The method presented in this work can be thought of as resulting from an approximation of a rate of change of stress that also incorporates rate of change of the convected coordinate system used to express it. Discretising the Oldroyd-B constitutive law with an appropriately chosen finite difference methods provides a natural way to preserve positive definiteness of the conformation tensor. To our knowledge, the idea of conducting computations for viscoelastic fluids by discretising the upper convected derivative expressed as a Lie derivative was first proposed in [35]. Theory was developed in [25, 26] for a finite element method in the framework of Riccati equations. A finite difference scheme for the Oldroyd-B constitutive law with prescribed velocity field was presented with truncation analysis in [30]. These methods can be viewed as an extension of characteristic schemes, which are well established in fluid dynamics due to their favourable stability properties, see [37] for an early reference, with analysis of a finite element method given in [44]. For example, when applied to the transport equation, stable solutions are obtained even for large CFL numbers. These methods have also been used to discretise the advective part of the upper convected derivative in computations involving viscoelastic fluids [8].

The discretisation of this problem in the Lie derivative framework has distinct advantages and unique challenges. One of the goals of the paper is to compare these features with other common approaches, and to test the limits of Lie derivative discretisation methods. We present a scheme based upon the Lie derivative where the conformation tensor is evolved pointwise, and spatial discretisation enters only through the approximation of the deformation gradient tensor and particle trajectories and interpolation. We note that similar schemes have appeared in the literature [3, 25, 26, 30], but our aim in this work is to present results from a full implementation in a challenging test case that can be compared with other published data.

In this article, we provide an accessible overview of viscoelastic fluid dynamics, particularly focused on polymer solutions modeled by the Oldroyd-B constitutive law. We develop a numerically tractable scheme for the model and prove the well-posedness. Our developed scheme also performs favorably in comparison to more computationally intensive alternatives that typically require high performance computing to realise. A thorough comparative study is presented, demonstrating the robustness of our approach. Furthermore, we discuss appropriate mesh design critical for capturing the complex dynamics of viscoelastic flows. This article will focus on the lid-driven cavity problem: a challenging test problem for non-Newtonian flows due to strong shearing that occurs near the moving lid, as well as strong stress gradients at the corners. It is a well-studied benchmark test case in the numerical literature on simulation of the Oldroyd-B model [7, 10, 16, 19, 34, 43], and serves as a useful example to illustrate key differences between Newtonian and non-Newtonian flows.

The outline of the rest of the article is as follows. In §2, we describe the Oldroyd-B model. Key concepts from continuum mechanics are introduced in §3, where a reformulation of the upper convected time derivative is described. In §4, a semidiscrete upper convected time derivative is introduced, and its consistency and approximation order is given. We discuss fully discrete numerical methods in §5. We work with a decoupled formulation, and so we discuss solution of the Stokes and Oldroyd-B systems separately. Descriptions of

computational aspects and implementation details, as well as numerical experiments are presented in §6.

2 The Oldroyd-B model

Let $\Omega \subset \mathbb{R}^d$ be a convex domain with polygonal boundary, and let $\mathbf{u} : \Omega \times [0, T] \rightarrow \mathbb{R}^d$ be the spatial velocity field, with $p : \Omega \times [0, T] \rightarrow \mathbb{R}$ the pressure. The (symmetric) *conformation tensor* $\boldsymbol{\sigma} : \Omega \rightarrow \mathbb{R}^{d^2}$ describes the non-Newtonian component of the stress. We let $\boldsymbol{\varepsilon}(\mathbf{u})$ be the rate of strain tensor, or symmetrised velocity gradient:

$$\boldsymbol{\varepsilon}(\mathbf{u}) = \frac{1}{2} (\nabla \mathbf{u} + (\nabla \mathbf{u})^T).$$

The Oldroyd-B model for the flow of a fluid in Ω consists of the Navier-Stokes equations for incompressible flow given by

$$\begin{aligned} \text{Re} \left(\frac{\partial \mathbf{u}}{\partial t} + (\mathbf{u} \cdot \nabla) \mathbf{u} \right) &= -\nabla p + 2\beta \text{div}(\boldsymbol{\varepsilon}(\mathbf{u})) + \frac{1-\beta}{\text{Wi}} \text{div}(\boldsymbol{\sigma}) \\ \text{div} \mathbf{u} &= 0. \end{aligned} \tag{1}$$

This is coupled to a hyperbolic constitutive law for the evolution of the stress, and is given below in non-dimensional form.

$$\frac{\partial \boldsymbol{\sigma}}{\partial t} + (\mathbf{u} \cdot \nabla) \boldsymbol{\sigma} - (\nabla \mathbf{u}) \boldsymbol{\sigma} - \boldsymbol{\sigma} (\nabla \mathbf{u})^T = -\frac{1}{\text{Wi}} (\boldsymbol{\sigma} - \mathbf{I}). \tag{2}$$

The system has three parameters, namely the familiar Reynolds number Re , the elasticity ratio β and the *Weissenberg number*, Wi . The regime of interest in this work is low Re and high Wi . We will assume that $\beta > 0$ to avoid the complications that can arise from the viscous term being removed and the system becoming fully hyperbolic (these difficulties are discussed in more detail in [6]). We note that the conformation tensor is related to the polymeric extra-stress tensor $\boldsymbol{\tau}$ by

$$\boldsymbol{\sigma} = \mathbf{I} + \frac{\text{Wi}}{1-\beta} \boldsymbol{\tau}.$$

We note that in the context in this work (i.e. a lid-driven cavity), the Weissenberg and Deborah numbers are related to each other via the aspect ratio of the cavity [33], and are in fact equal for a cavity of square cross-section.

We prescribe Dirichlet boundary conditions \mathbf{w} on $\partial\Omega$ for the velocity such that $\mathbf{w} \cdot \mathbf{n} = 0$ on $\partial\Omega$, where \mathbf{n} is the outward facing normal vector to the boundary, i.e. the problem is driven by tangential boundary values for the velocity. We note that since Dirichlet boundary conditions are prescribed on the whole boundary, to ensure that there exists a uniquely determined pressure field we include the constraint that the pressure has mean zero. Initial conditions for the fluid velocity and conformation tensor are given by $\mathbf{u}(\mathbf{x}, 0) = \mathbf{u}^0(\mathbf{x})$ and $\boldsymbol{\sigma}(\mathbf{x}, 0) = \boldsymbol{\sigma}^0(\mathbf{x})$ respectively.

The left hand side of Equation (2) is the *upper convected time derivative*, introduced by Oldroyd [31] and discussed in greater detail in §3. See also [21] for an overview. It gives the rate of change of a tensor quantity in a convected coordinate system which moves and deforms with the fluid. Such a rate is appropriate to derive constitutive laws which exhibit material frame indifference that is, the principle that the physics of the constitutive law should be independent of the frame of the observer.

Remark 2.1 (Boundary conditions for the conformation tensor). *The problem described above is an enclosed flow. Since there is no inflow boundary, and since the constitutive relation (2) is hyperbolic, no boundary condition is required for the conformation tensor. The case of inflow boundary conditions for the velocity, which we do not consider here, requires additional boundary conditions for the conformation tensor. This is not a well studied problem and another potential source of instabilities in these flows.*

To complete the exposition, it is appropriate to discuss some of the assumptions made in the derivation of the Oldroyd-B model. The introduction of the upper convected time derivative by Oldroyd [31] assumes that the physics of the constitutive relation are formulated in terms of the evolution of contravariant components of a second order tensor in the convected frame moving and deforming with the fluid. This is a choice, justified by experiments exhibiting rod-climbing (a phenomenon that the Oldroyd-B model replicates), rather than physics, and other choices may be more appropriate (see the discussion in [21]).

The model has also been derived from kinetics using a dumbbell and spring model in which no limit is placed upon the extension of the spring. However, if the flow is strong (that is, if the largest eigenvalue of $\nabla \mathbf{u}$ exceeds $\frac{1}{2\lambda}$, where λ is the relaxation time [21]), the molecule length increases without limit. It has been shown that, as a result of this, infinite stress can occur in the interior of a steady flow. In many regimes however, the Oldroyd-B fluid is a good approximation of a Boger fluid. It is the simplest differential viscoelastic model available which enjoys material frame indifference (simpler models do exist such as the linear Maxwell model, see [39, Chapter 2] for an overview, but do not have this property). It is also popular, with a wide range of benchmark numerical data available in the literature. It therefore represents a prototypical model for the derivation and testing of numerical methods, see for example [16, 24, 26, 29, 36] and many others.

Remark 2.2. *Taking the kinetic viewpoint, the Oldroyd-B model can be improved by considering for example variants of the Finitely Extensible Nonlinear Elastic (FENE) model for the spring force in the polymer molecules, which limits molecules to be finitely extensible and avoiding the issue of unbounded stress growth. This does however result in a more complicated nonlinearity in the constitutive law. For example, the FENE-P model has constitutive law given by*

$$\frac{\partial \boldsymbol{\sigma}}{\partial t} + (\mathbf{u} \cdot \nabla) \boldsymbol{\sigma} - (\nabla \mathbf{u}) \boldsymbol{\sigma} - \boldsymbol{\sigma} (\nabla \mathbf{u})^T = \frac{1}{\text{Wi}} \left(\mathbf{I} - \frac{1}{1 - \frac{1}{b^2} \text{tr}(\boldsymbol{\sigma})} \boldsymbol{\sigma} \right),$$

where the additional parameter b represents the maximum extensibility of the polymer molecules. The extension of the current work to more realistic models will be the subject of further research.

3 A Lie derivative framework for the upper convected time derivative

In his seminal paper [31], Oldroyd described the importance of formulating a time derivative with which to construct constitutive laws for non-Newtonian stresses that does not depend on the choice of reference frame. Such derivatives have to take account of the moving fluid flow and its deformation. The *upper convected time derivative*, one of two derivatives introduced by Oldroyd, is one of (infinitely) many such time derivatives. It is now well known that these rates are special cases of Lie derivatives (see eg [22, chapter II]), and formulating

the constitutive law in a way that respects this can have structure-preserving advantages. In this section we give the concepts necessary to formulate the constitutive law for a non-Newtonian fluid as a Lie derivative.

3.1 Flow map and deformation gradient

Let \mathbf{y} be the flow map for the fluid motion. That is, the fluid particle which at time t has position \mathbf{x} has position $\mathbf{y}(\mathbf{x}, t; s)$ at time s . The flow map satisfies the following ordinary differential equation

$$\begin{aligned}\partial_s \mathbf{y}(\mathbf{x}, t; s) &= \mathbf{u}(\mathbf{y}(\mathbf{x}, t; s), s) \\ \mathbf{y}(\mathbf{x}, t; t) &= \mathbf{x}.\end{aligned}$$

One can express the material derivative in terms of the flow map by examining the infinitesimal derivative, that is

$$\left. \frac{\partial}{\partial s} \mathbf{u}(\mathbf{y}(\mathbf{x}, t; s), s) \right|_{s=t} = (\partial_t + \mathbf{u} \cdot \nabla) \mathbf{u}(\mathbf{x}, t).$$

We define the velocity gradient with the convention that it has components

$$(\nabla \mathbf{u})_{ij} = \frac{\partial u_i}{\partial x_j},$$

and make note that some authors define the velocity gradient as the transpose of the above tensor. The deformation gradient tensor describes the deformation experienced by a fluid parcel in a neighbourhood of (\mathbf{x}, t) between times s_1 and s_2 . In a Cartesian coordinate system, it has components

$$\mathbf{F}_{ij}(\mathbf{x}, t; s_1, s_2) = \frac{\partial \mathbf{y}_i(\mathbf{x}, t; s_2)}{\partial \mathbf{y}_j(\mathbf{x}, t; s_1)}. \quad (3)$$

It can alternatively be expressed in the following way:

$$\mathbf{F}(\mathbf{x}, t; t, s) = \nabla \mathbf{y}(\mathbf{x}, t; s).$$

Where no confusion can occur, we will omit the particle label and for brevity write $\mathbf{F}(s_1, s_2)$ for $\mathbf{F}(\mathbf{x}, t; s_1, s_2)$ and $\mathbf{y}(s)$ for $\mathbf{y}(\mathbf{x}, t; s)$.

It follows immediately from the definition that $\mathbf{F}(s, s) = \mathbf{I}$, where \mathbf{I} is the identity tensor, and that $\mathbf{F}(s_1, s_2) = \mathbf{F}(s_2, s_1)^{-1}$. The deformation gradient is a two point tensor, and the following lemma describes its evolution with respect to the two faux time indices:

Lemma 3.1 (Evolution of the deformation gradient along characteristics). *The deformation gradient tensor satisfies the following differential equations.*

$$\frac{\partial}{\partial s_1} \mathbf{F}(\mathbf{x}, t; s_1, s_2) = -\mathbf{F}(\mathbf{x}, t; s_1, s_2) \nabla \mathbf{u}(\mathbf{y}(\mathbf{x}, t; s_1), s_1) \quad (4)$$

$$\frac{\partial}{\partial s_2} \mathbf{F}(\mathbf{x}, t; s_1, s_2) = \nabla \mathbf{u}(\mathbf{y}(\mathbf{x}, t; s_2), s_2) \mathbf{F}(\mathbf{x}, t; s_1, s_2). \quad (5)$$

Proof. We begin with Equation (3) and use the chain rule to compute the components of $\partial_{s_2} \mathbf{F}(s_1, s_2)$:

$$\begin{aligned} \frac{\partial}{\partial s_2} \mathbf{F}(s_1, s_2)_{ij} &= \frac{\partial}{\partial s_2} \left(\frac{\partial \mathbf{y}_i(s_2)}{\partial \mathbf{y}_j(s_1)} \right) = \frac{\partial \mathbf{u}_i(\mathbf{y}(s_2), s_2)}{\partial \mathbf{y}_j(s_1)} = \frac{\partial \mathbf{u}_i(\mathbf{y}(s_2), s_2)}{\partial \mathbf{y}_k(s_2)} \frac{\partial \mathbf{y}_k(s_2)}{\partial \mathbf{y}_j(s_1)} \\ &= \nabla \mathbf{u}(\mathbf{y}(s_2), s_2)_{ik} \mathbf{F}(s_1, s_2)_{kj}, \end{aligned}$$

showing (5). The proof of (4) follows in a similar manner. \square

Proposition 3.2. *The determinant of the deformation gradient \mathbf{F} is an invariant of Equations (4) and (5). In particular, $\det(\mathbf{F}(s_1, s_2)) = 1$ for all s_1, s_2 .*

Proof. For any s , we have $\det(\mathbf{F}(s, s)) = \det(\mathbf{I}) = 1$. Now, (5) is a tensor-valued differential equation with coefficient matrix $\nabla \mathbf{u}(\mathbf{y}(s_2), s_2)$. Since the fluid is incompressible, the trace of the velocity gradient is zero. We can therefore invoke [20, §IV.3, Lemma 3.1] which guarantees $\det(\mathbf{F}(s_1, s_2))$ is invariant. \square

3.2 The upper convected time derivative

For a generic sufficiently smooth tensor function $\boldsymbol{\zeta}$, the upper convected derivative is defined through

$$\overset{\nabla}{\boldsymbol{\zeta}} := \frac{\partial \boldsymbol{\zeta}}{\partial t} + (\mathbf{u} \cdot \nabla) \boldsymbol{\zeta} - (\nabla \mathbf{u}) \boldsymbol{\zeta} - \boldsymbol{\zeta} (\nabla \mathbf{u})^T.$$

This has a relationship to the notion of a *Lie derivative* of the tensor quantity $\boldsymbol{\zeta}$ which we will exploit in this work. Indeed, one may introduce the Lie derivative which follows the fluid with deformation gradient tensor \mathbf{F} by

$$(\mathcal{L}_u \boldsymbol{\zeta})(\mathbf{y}(\mathbf{x}, t; s), s) := \mathbf{F}(t, s) \frac{\partial}{\partial s} [\mathbf{F}(s, t) \boldsymbol{\zeta}(\mathbf{y}(s), s) \mathbf{F}(s, t)^T] \mathbf{F}(t, s)^T.$$

The upper-convected derivative can be inferred from the fundamental properties of \mathbf{F} given in §3.1 [25, 30]

$$\overset{\nabla}{\boldsymbol{\zeta}} = \lim_{s \rightarrow t} (\mathcal{L}_u \boldsymbol{\zeta})(\mathbf{y}(\mathbf{x}, t; s), s).$$

The Oldroyd-B constitutive relation for the conformation tensor can therefore be formulated in terms of the Lie derivative resulting in an equation in one (characteristic) time variable as follows

$$\overset{\nabla}{\boldsymbol{\sigma}} = \lim_{s \rightarrow t} (\mathcal{L}_u \boldsymbol{\sigma})(\mathbf{y}(\mathbf{x}, t; s), s) = -\frac{1}{\text{Wi}} (\boldsymbol{\sigma} - \mathbf{I}). \quad (6)$$

We see that the constitutive law in Oldroyd-B is a linear ODE along the characteristics induced by the deformation gradient \mathbf{F} . This is why Oldroyd-B is often referred to as a linear viscoelastic model. It also offers the opportunity to utilise a wide variety of timestepping methods designed for problems of this kind.

4 Discretisation of the upper convected time derivative

In this section we introduce a discretisation of the upper convected time derivative motivated by its formulation as a Lie derivative given in §3. The method will be similar to characteristic schemes, where the

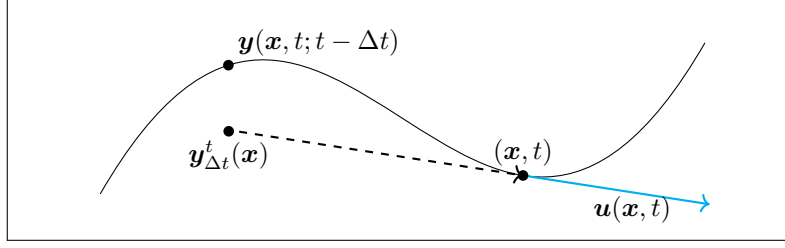


Figure 1: Graphical illustration of the departure point $y(x, t; t - \Delta t)$ of (x, t) under the flow map, and the approximate departure point $y_{\Delta t}^t(x)$. The curve represents the characteristic that the particle (x, t) belongs to.

material derivative is discretised along the characteristics of the flow [37, 41, 44]. Adapting this methodology to account for the deformation of the fluid provides a natural way to preserve the positive definiteness of the conformation tensor of any given discretisation. This idea has been explored previously in the context of several different numerical frameworks [8, 26, 30, 35].

We divide the time domain $[0, T]$ into a uniform partition of N subintervals of length Δt (so that $T = N\Delta t$). We write $t^n = n\Delta t$ for $n = 0, 1, \dots, N$, non uniform timestepping is certainly possible however for clarity of exposition we will restrict to uniform. We also use the notation $u^n(x) = u(x, t^n)$. Starting from

$$(\mathcal{L}_u \zeta)(y(x, t; s), s) = F(t, s) \frac{\partial}{\partial s} [F(s, t) \zeta(y(s), s) F(s, t)^T] F(t, s)^T, \quad (7)$$

we will utilise a finite difference approach which motivates the following definitions:

Definition 4.1 (Semidiscrete upper convected derivative). *For $x \in \Omega$, $0 < \Delta t < T$ and $t \in [\Delta t, T]$, define*

$$y_{\Delta t}^t(x) = x - \Delta t u(x, t), \quad (8)$$

as an approximation of the departure point of x under the fluid velocity at time t . Further, let

$$F_{\Delta t}^t(x) = I + \Delta t \nabla u(x, t), \quad (9)$$

denote an approximation of the deformation gradient tensor between times $t - \Delta t$ and t . We define a discrete upper-convected time derivative of a generic, sufficiently smooth, tensor function ζ by the velocity field $u(x, t)$ as

$$D_{(u, \Delta t)} \zeta(x, t) = \frac{1}{\Delta t} \left(\zeta(x, t) - F_{\Delta t}^t(x) \zeta(y_{\Delta t}^t, t - \Delta t) F_{\Delta t}^t(x)^T \right).$$

Remark 4.2. *Different choices are available to make this approximation depending on the desired properties of the scheme. Definition 4.1 results from choosing a backward Euler discretisation, whereby the right hand side of Equation (7) is approximated by*

$$F(t, s) \frac{1}{\Delta t} \left\{ F(s, t) \zeta(y(s), s) F(s, t)^T - F(s - \Delta t, t) \zeta(y(s - \Delta t), s - \Delta t) F(s - \Delta t, t)^T \right\} F(t, s)^T,$$

which after evaluating at $s = t$ becomes

$$\frac{1}{\Delta t} \{ \boldsymbol{\zeta}(\mathbf{x}, t) - \mathbf{F}(t - \Delta t, t) \boldsymbol{\zeta}(\mathbf{y}(t - \Delta t), t - \Delta t) \mathbf{F}(t - \Delta t, t)^T \}. \quad (10)$$

It is not always practical (or possible) to exactly evaluate the deformation gradient and flow map, so they are replaced with approximations $\mathbf{F}_{\Delta t}^t$ and $\mathbf{y}_{\Delta t}^t$ respectively in the definition of $D_{(\mathbf{u}, \Delta t)}$.

The structure associated to (6) is dissipative in nature hence a BDF discretisation is quite natural. A detailed discussion of approximations of the upper convected time derivative in the manner described above is given in [30], where the authors discuss first and second order approximations of BDF type.

We now turn our attention to well-posedness and properties of the scheme. We first show in Lemma 4.3 that $D_{(\mathbf{u}, \Delta t)}$ is well-defined as long as Δt is chosen to be sufficiently small. For a velocity \mathbf{u} satisfying a homogeneous Dirichlet boundary condition, this result is proved in [41]. We provide an extension of that result appropriate for nonzero tangential velocity boundary conditions such as the lid-driven cavity.

Lemma 4.3. *Let Ω be the unit square or the unit cube. Assume that $\mathbf{u} \cdot \mathbf{n} = 0$ on $\partial\Omega$, and that Δt is chosen so that $\Delta t \|\mathbf{u}\|_{C^0([0, T]; W^{1, \infty}(\Omega))} < 1$. Then for any $\mathbf{x} \in \Omega$, and any $t \in [\Delta t, T]$, we have $\mathbf{y}_{\Delta t}^t(\mathbf{x}) \in \Omega$.*

Proof. Let $\mathbf{x} \in \Omega$. Then, by (8)

$$|\mathbf{x} - \mathbf{y}_{\Delta t}^t(\mathbf{x})| = \Delta t |\mathbf{u}(\mathbf{x}, t)|.$$

The boundary of Ω has the form $\partial\Omega = \cup_{i=1} \Gamma_i$ where Γ_i is a line segment when $d = 2$ and a plane segment when $d = 3$. Let $\mathbf{x} \in \Omega$ and for some i , denote by \mathbf{x}_{Γ_i} the unique point on Γ_i that satisfies $|\mathbf{x} - \mathbf{x}_{\Gamma_i}| = \text{dist}(\mathbf{x}, \Gamma_i)$. As Ω is convex this point clearly lies in the interior of Γ_i , so that the unit outward normal to the boundary at \mathbf{x}_{Γ_i} is well-defined, and the line segment joining \mathbf{x} and \mathbf{x}_{Γ_i} is perpendicular to Γ_i . We consider the component of the velocity in the direction of $\mathbf{n}(\mathbf{x}_{\Gamma_i})$. Since $\mathbf{u}(\mathbf{x}_{\Gamma_i}, t) \cdot \mathbf{n}(\mathbf{x}_{\Gamma_i}) = 0$,

$$\begin{aligned} \mathbf{u}(\mathbf{x}, t) \cdot \mathbf{n}(\mathbf{x}_{\Gamma_i}) &= \int_0^1 \frac{\partial}{\partial s} \mathbf{u}(\mathbf{x}_{\Gamma_i} + s(\mathbf{x} - \mathbf{x}_{\Gamma_i}), t) \cdot \mathbf{n}(\mathbf{x}_{\Gamma_i}) \, ds, \\ &= (\mathbf{x} - \mathbf{x}_{\Gamma_i}) \cdot \int_0^1 \nabla \mathbf{u}(\mathbf{x}_{\Gamma_i} + s(\mathbf{x} - \mathbf{x}_{\Gamma_i}), t) \cdot \mathbf{n}(\mathbf{x}_{\Gamma_i}) \, ds \\ &\leq \text{dist}(\mathbf{x}, \Gamma_i) \|\mathbf{u}\|_{C^0([0, T]; W^{1, \infty}(\Omega))}, \end{aligned}$$

where $\mathbf{n}(\mathbf{x}_{\Gamma_i})$ is the unit normal to $\partial\Omega$ at \mathbf{x}_{Γ_i} . Again, using (8) we have shown that

$$|(\mathbf{x} - \mathbf{y}_{\Delta t}^t(\mathbf{x})) \cdot \mathbf{n}(\mathbf{x}_{\Gamma_i})| \leq \text{dist}(\mathbf{x}, \Gamma_i) \Delta t \|\mathbf{u}\|_{C^0([0, T]; W^{1, \infty}(\Omega))} \leq \text{dist}(\mathbf{x}, \Gamma_i),$$

that is, the velocity at \mathbf{x} in the direction of $\mathbf{n}(\mathbf{x}_{\Gamma_i})$ is not large enough for the line segment joining \mathbf{x} and $\mathbf{y}_{\Delta t}^t(\mathbf{x})$ to cross Γ_i . Since the choice of i was arbitrary, we must have that $\mathbf{y}_{\Delta t}^t(\mathbf{x}) \in \Omega$. \square

In the following lemmata, we discuss the approximation properties of $\mathbf{y}_{\Delta t}^t$, $\mathbf{F}_{\Delta t}^t$ and finally $D_{(\mathbf{u}, \Delta t)}$. We will utilise certain results which were proved in [30]. The first, Lemma 4.4, gives a bound on the error arising from approximating the departure point using (8) (see Figure 1 for an illustration), while Lemma 4.5 bounds the error in evaluating a tensor function at this approximate departure point as opposed to the true point. The error in approximating the deformation gradient is bounded in Lemma 4.6, and finally a bound

showing the consistency and approximation order of the discrete upper convected derivative $D_{(\mathbf{u}, \Delta t)}$ is given in Theorem 4.8.

Lemma 4.4 (Approximation of characteristics [30, Lemma 2]). *Suppose that $\mathbf{u} \cdot \mathbf{n} = 0$ on $\partial\Omega$ and that $\Delta t \|\mathbf{u}\|_{C^0([0,T];W^{1,\infty}(\Omega))} < 1$. Then for any $\mathbf{x} \in \Omega$ and $t \geq \Delta t$,*

$$\mathbf{y}(\mathbf{x}, t; t - \Delta t) - \mathbf{y}_{\Delta t}^t(\mathbf{x}) = \frac{\Delta t^2}{2} \frac{D\mathbf{u}}{Dt} + \mathcal{O}(\Delta t^3). \quad (11)$$

Lemma 4.5. *In addition to the hypotheses of Lemma 4.4, let ζ be an appropriately differentiable tensor function. Then for any $\mathbf{x} \in \Omega$ and $t \geq \Delta t$,*

$$\zeta(\mathbf{y}(\mathbf{x}, t; t - \Delta t), t - \Delta t) - \zeta(\mathbf{y}_{\Delta t}^t(\mathbf{x}), t - \Delta t) = \frac{\Delta t^2}{2} \left(\frac{D\mathbf{u}}{Dt} \cdot \nabla \right) \zeta + \mathcal{O}(\Delta t^3).$$

Lemma 4.6 (Approximation of deformation gradient [30, Lemma 1]). *Suppose that the hypotheses of Lemma 4.4 are satisfied. Then for any $\mathbf{x} \in \Omega$ and $t \geq \Delta t$,*

$$\mathbf{F}(t - \Delta t, t) - \mathbf{F}_{\Delta t}^t(\mathbf{x}) = \Delta t^2 \left[(\nabla \mathbf{u})^2 - \frac{D(\nabla \mathbf{u})}{Dt} \right] + \mathcal{O}(\Delta t^3).$$

Remark 4.7. *The bounds of Lemma 4.4 and Lemma 4.6 require spatial and temporal regularity of \mathbf{u} due for example to the appearance of the material derivative of \mathbf{u} on the right hand side of Equation (11). In addition, the result of Lemma 4.5 requires spatial regularity of ζ .*

We finally arrive at the approximation of the upper convected derivative (see [30, Remark 7]).

Theorem 4.8. *Suppose that the hypotheses of Lemma 4.4 are satisfied, and that ζ is an appropriately differentiable tensor function. Then for any $\mathbf{x} \in \Omega$ and $t \geq \Delta t$,*

$$\overset{\nabla}{\zeta}(\mathbf{x}, t) = D_{(\mathbf{u}, \Delta t)} \zeta(\mathbf{x}, t) + \mathcal{O}(\Delta t).$$

Theorem 4.8 may be interpreted as an expansion around \mathbf{x}, t in that it follows directly that we have, at $\mathbf{y}_{\Delta t}^t(\mathbf{x})$,

$$\mathbf{F}_{\Delta t}^t(\mathbf{x}) \zeta(\mathbf{y}_{\Delta t}^t, t - \Delta t) \mathbf{F}_{\Delta t}^t(\mathbf{x})^T = \zeta(\mathbf{x}, t) - \Delta t \overset{\nabla}{\zeta}(\mathbf{x}, t) + \mathcal{O}(\Delta t^2).$$

We are now in a position to state the semidiscrete scheme for the constitutive law (2).

4.1 Semidiscretisation of the Oldroyd-B constitutive law

Suppose that $\mathbf{u}(\mathbf{x}, t)$ is given for $\mathbf{x} \in \Omega$ and $t \in [0, T]$. Suppose also that an initial condition $\boldsymbol{\sigma}^0(\mathbf{x})$ is given. Then for $n \geq 1$ we define $\boldsymbol{\Sigma}^n$ by

$$\begin{aligned} D_{(\mathbf{u}, \Delta t)} \boldsymbol{\Sigma}^n(\mathbf{x}) &= -\frac{1}{\text{Wi}} (\boldsymbol{\Sigma}^n(\mathbf{x}) - \mathbf{I}) \\ \boldsymbol{\Sigma}^0(\mathbf{x}) &= \boldsymbol{\sigma}^0(\mathbf{x}). \end{aligned} \quad (12)$$

Proposition 4.9 (Consistency). *The semidiscrete scheme given in (12) is a consistent, first order approximation.*

Proof. By Theorem 4.8, we have the following representation:

$$\boldsymbol{\sigma}(\mathbf{x}, t) = \Delta t \overset{\nabla}{\boldsymbol{\sigma}}(\mathbf{x}, t) + \mathbf{F}_{\Delta t}^t(\mathbf{x}) \boldsymbol{\sigma}(\mathbf{y}_{\Delta t}^t(\mathbf{x}), t - \Delta t) \mathbf{F}_{\Delta t}^t(\mathbf{x})^T + \mathcal{O}(\Delta t^2).$$

Then, using Equation (2), we obtain

$$\left(1 + \frac{\Delta t}{\text{Wi}}\right) \boldsymbol{\sigma}(\mathbf{x}, t) = \mathbf{F}_{\Delta t}^t(\mathbf{x}) \boldsymbol{\sigma}(\mathbf{y}_{\Delta t}^t(\mathbf{x}), t - \Delta t) \mathbf{F}_{\Delta t}^t(\mathbf{x})^T - \frac{\Delta t}{\text{Wi}} \mathbf{I} + \mathcal{O}(\Delta t^2). \quad (13)$$

Assuming that $\boldsymbol{\sigma}(\mathbf{y}_{\Delta t}^t(\mathbf{x}), t - \Delta t)$ is given, one step of the semidiscrete scheme gives that $\boldsymbol{\Sigma}^n$ satisfies

$$\left(1 + \frac{\Delta t}{\text{Wi}}\right) \boldsymbol{\Sigma}^n(\mathbf{x}) = \mathbf{F}_{\Delta t}^t(\mathbf{x}) \boldsymbol{\sigma}(\mathbf{y}_{\Delta t}^t(\mathbf{x}), t - \Delta t) \mathbf{F}_{\Delta t}^t(\mathbf{x})^T - \frac{\Delta t}{\text{Wi}} \mathbf{I}. \quad (14)$$

Finally, noting that for any $\Delta t > 0$, we have $0 < \frac{\text{Wi}}{\text{Wi} + \Delta t} < 1$, so that subtracting (14) from (13) gives

$$\boldsymbol{\sigma}(\mathbf{x}, t) - \boldsymbol{\Sigma}^n(\mathbf{x}) = \mathcal{O}(\Delta t^2),$$

and therefore the semidiscrete scheme has local truncation error proportional to Δt^2 . \square

Proposition 4.10 (The positive definiteness of the conformation tensor is preserved). *Suppose that $\boldsymbol{\Sigma}^{n-1}$ is given, and is positive definite, and assume that \mathbf{u} is given. Then there exists $\Delta t > 0$ such that $\boldsymbol{\Sigma}^n$ is positive definite.*

Proof. We can write (12) as

$$\left(1 + \frac{\Delta t}{\text{Wi}}\right) \boldsymbol{\Sigma}^n(\mathbf{x}) = \mathbf{F}_{\Delta t}^t(\mathbf{x}) \boldsymbol{\Sigma}^{n-1}(\mathbf{y}_{\Delta t}^t(\mathbf{x})) \mathbf{F}_{\Delta t}^t(\mathbf{x})^T + \frac{\Delta t}{\text{Wi}} \mathbf{I}. \quad (15)$$

Thus, as long as Δt is chosen small enough, a sufficient condition would be $\Delta t \leq \frac{1}{2} \|\mathbf{u}\|_{1,\infty}$ for example, $\mathbf{F}_{\Delta t}^t$ is invertible by the Gershgorin circle theorem [18, Thm 7.2.1]. Let $\mathbf{0} \neq \boldsymbol{\xi} \in \mathbb{R}^d$. Then since $\mathbf{F}_{\Delta t}^t$ is invertible, the product $(\mathbf{F}_{\Delta t}^t)^T \boldsymbol{\xi}$ is a nonzero vector in \mathbb{R}^d , so that by hypothesis

$$0 < \boldsymbol{\xi}^T \mathbf{F}_{\Delta t}^t \boldsymbol{\Sigma}^{n-1}(\mathbf{y}_{\Delta t}^t(\mathbf{x})) (\mathbf{F}_{\Delta t}^t)^T \boldsymbol{\xi}.$$

Then from (15), $\boldsymbol{\Sigma}^n(\mathbf{x})$ is a sum of two positive definite terms. \square

5 Spatial discretisation

In this section we present numerical methods for the Oldroyd-B fluid in the case $\text{Re} = 0$. The problem is solved in a decoupled manner, in which at each time step a Stokes problem is solved for the fluid velocity, which is then used as a forcing in the time-dependent constitutive relation. This avoids the need to solve a very large monolithic system and therefore keeps computational costs down. We first give a finite ele-

ment method to solve the Stokes problem and discuss well-posedness. We then present the fully discrete constitutive law and discuss the solution procedure for the full problem.

5.1 Finite element discretisation for the Stokes problem

We consider \mathcal{T} to be a conforming triangulation of Ω , namely, \mathcal{T} is a finite family of sets such that

1. $K \in \mathcal{T}$ implies K is an open box (i.e. a quadrilateral or hexahedron),
2. for any $K, J \in \mathcal{T}$ we have that $\overline{K} \cap \overline{J}$ is a full lower-dimensional box (i.e., it is either \emptyset , a vertex, an edge (or face) or the whole of \overline{K} and \overline{J}) of both \overline{K} and \overline{J} and
3. $\bigcup_{K \in \mathcal{T}} \overline{K} = \overline{\Omega}$.

Further, we define $h : \Omega \rightarrow \mathbb{R}$ to be the piecewise constant *meshsize function* of \mathcal{T} given by

$$h(\mathbf{x}) := \max_{\overline{K} \ni \mathbf{x}} \text{diam}(K).$$

With $\mathbb{Q}_1(K)$ the space of bilinear polynomials over a quadrilateral (or trilinear over a hexahedron), we introduce the *finite element space*

$$\mathbb{Q}_1 := \{\phi \in H^1(\Omega) : \phi|_K \in \mathbb{Q}_1(K)\},$$

to be the usual space of continuous piecewise bilinear functions. Let the vertices of the triangulation \mathcal{T} be denoted \mathbf{x}_i . For a vertex \mathbf{x}_i , we define

$$\hat{\mathbf{x}}_i := \{K \in \mathcal{T} : \mathbf{x}_i \in \overline{K}\}.$$

To facilitate strong imposition of boundary conditions for the velocity, we introduce finite element spaces

$$\mathbb{V}_{\mathbf{w}} := \{\mathbf{v} \in \mathbb{Q}_1^d : \mathbf{v}|_{\partial\Omega} = \Pi_1 \mathbf{w}\}$$

$$\mathbb{V}_{\mathbf{0}} := \{\mathbf{v} \in \mathbb{Q}_1^d : \mathbf{v}|_{\partial\Omega} = \mathbf{0}\}.$$

To solve the Stokes problem, we employ the stabilised equal-order approximation introduced in [12]. The stabilisation makes use of the L^2 projection operator $\Pi_0 : \mathbb{Q}_1 \rightarrow \mathbb{P}_0$ that maps the finite element space to a space of discontinuous functions which are constant on each element. The construction of the stabilisation term is therefore local to elements. In addition, this scheme performs well on graded meshes, which are a useful tool due to the sharp boundary layers that occur in viscoelastic fluid flows (see §6.2). A more detailed discussion and analysis for this scheme can be found in [5, 12, 14]. Let $\boldsymbol{\Sigma}_h^0$ be a given interpolant of $\boldsymbol{\Sigma}^0$. Then the discrete problem for the velocity and pressure is to find $\mathbf{u}_h \in \mathbb{V}_{\mathbf{w}}, p_h \in \mathbb{Q}_1$ such that

$$2\beta \int_{\Omega} \boldsymbol{\varepsilon}(\mathbf{u}_h) : \boldsymbol{\varepsilon}(\mathbf{v}_h) - \int_{\Omega} p_h \text{div } \mathbf{v}_h - \int_{\Omega} q_h \text{div } \mathbf{u}_h - \int_{\Omega} (p_h - \Pi_0 p_h)(q_h - \Pi_0 q_h) = \frac{\beta - 1}{\text{Wi}} \int_{\Omega} \boldsymbol{\Sigma}_h^0 : \boldsymbol{\varepsilon}(\mathbf{v}_h) \quad (16)$$

for all $\mathbf{v}_h \in \mathbb{V}_{\mathbf{0}}, q_h \in \mathbb{Q}_1$.

Proposition 5.1 (Inf-sup stability [5]). *Let*

$$B_h((\mathbf{u}_h, p_h), (\mathbf{v}_h, q_h)) := 2\beta \int_{\Omega} \boldsymbol{\varepsilon}(\mathbf{u}_h) : \boldsymbol{\varepsilon}(\mathbf{v}_h) - \int_{\Omega} p_h \operatorname{div} \mathbf{v}_h - \int_{\Omega} q_h \operatorname{div} \mathbf{u}_h - \int_{\Omega} (p_h - \Pi_0 p_h)(q_h - \Pi_0 q_h). \quad (17)$$

Then, there exists a $C > 0$ independent of h such that

$$\sup_{\mathbf{v}_h \in \mathbb{Q}_1^d, q_h \in \mathbb{Q}_1} \frac{B_h((\mathbf{u}_h, p_h), (\mathbf{v}_h, q_h))}{\|\mathbf{v}_h\|_{\mathbf{H}^1(\Omega)} + \|q_h\|_{L^2(\Omega)}} \geq C \left(\|\mathbf{u}_h\|_{\mathbf{H}^1(\Omega)} + \|p_h\|_{L^2(\Omega)} \right) \quad \forall \mathbf{u}_h \in \mathbb{Q}_1^d, p_h \in \mathbb{Q}_1. \quad (18)$$

The inf-sup condition guarantees that problem (16) is well-posed.

5.2 A finite difference approximation of the upper convected time derivative

The discretisation of the constitutive law requires several definitions relating to approximations of characteristics and deformation gradients, which we now give. We write \mathbf{u}_h^n for the discrete solution at time t^n .

Remark 5.2. *If we assume $\mathbf{u} \in W^{1,\infty}(\Omega) \cap H^2(\Omega)$ then standard arguments can be used to infer the discrete velocity $\mathbf{u}_h^n \in W^{1,\infty}(\Omega)$. Also since $\mathbf{u}_h^n \cdot \mathbf{n} = 0$ on $\partial\Omega$ we have, in light of Lemma 4.3, the approximation (20) is also well-defined.*

Definition 5.3. *Let $\mathbf{u}_h^n \in \mathbb{Q}_1^d$ be given. For any $\mathbf{x} \in \Omega$ and $n \geq 1$, define the discrete departure point of \mathbf{x} according to the velocity \mathbf{u}_h^n as*

$$\mathbf{y}_{h,\Delta t}^n(\mathbf{x}) = \mathbf{x} - \Delta t \mathbf{u}_h^n(\mathbf{x}). \quad (19)$$

We also define the discrete deformation gradient between time $(n-1)\Delta t$ and $n\Delta t$ as

$$\mathbf{F}_{h,\Delta t}^n = \mathbf{I} + \Delta t \nabla \mathbf{u}_h^n(\mathbf{x}).$$

Definition 5.4 (Fully discrete approximate upper convected time derivative). *Let \mathbf{u}_h^n be given, and suppose that $\boldsymbol{\zeta}^{n-1}, \boldsymbol{\zeta}^n$ are tensor valued functions representing the value of a time dependent tensor field at the time levels $n-1, n$. Then the fully discrete approximation to the upper convected time derivative of $\boldsymbol{\zeta}$ at time level n is given by*

$$D_{(\mathbf{u}_h^n, \Delta t)}^h \boldsymbol{\zeta}^n(\mathbf{x}) := \frac{1}{\Delta t} \left(\boldsymbol{\zeta}^n(\mathbf{x}) - \mathbf{F}_{h,\Delta t}^n(\mathbf{x}) \boldsymbol{\zeta}^{n-1}(\mathbf{y}_{h,\Delta t}^n(\mathbf{x})) \mathbf{F}_{h,\Delta t}^n(\mathbf{x})^T \right). \quad (20)$$

5.3 A fully discrete scheme for the Stokes flow of an Oldroyd-B fluid

We are now in a position to define the full finite difference discretisation of the constitutive law. Values of the discrete conformation tensor are stored at the vertices \mathbf{x}_i . At any time level k , these values are sufficient to uniquely define a function $\boldsymbol{\Sigma}_h^k \in \mathbb{Q}_1^{d(d+1)/2}$ by bilinear (or trilinear) interpolation. This representation is used to evaluate the conformation tensor at points which are not vertices, and is the function on the right hand side of the discrete Stokes equation (16). By a slight abuse of notation, we will write $\boldsymbol{\Sigma}_h^k$ for both the set of point values at vertices, and the function in $\mathbb{Q}_1^{d(d+1)/2}$ obtained by interpolation using these values.

We note that the approximation of the deformation gradient needed to evaluate (20) requires the value of the discrete velocity gradient, which we wish to use at the vertices of the mesh. Since the discrete velocity lies in \mathbb{Q}_1^d , the point values of its gradient are not well defined. For a vertex \mathbf{x}_i of the mesh and a function $\mathbf{v}_h \in \mathbb{Q}_1^d$, in place of the velocity gradient, we therefore use the local average over $\hat{\mathbf{x}}_i$:

$$\nabla \mathbf{v}_h(\mathbf{x}_i) = \frac{1}{|\hat{\mathbf{x}}_i|} \sum_{K \subseteq \hat{\mathbf{x}}_i} \int_K \nabla \mathbf{v}_h.$$

The fully discrete problem is given as follows. Let Σ_h^0 be an interpolant of the initial condition. Then for $1 \leq n \leq N$, find $\mathbf{u}_h^n \in \mathbb{V}_w$, $p_h^n \in \mathbb{Q}_1$ such that

$$B_h((\mathbf{u}_h^n, p_h^n), (\mathbf{v}_h, q_h)) = \frac{\beta - 1}{\text{Wi}} \int_{\Omega} \Sigma_h^{n-1} : \varepsilon(\mathbf{v}_h) \quad (21)$$

for all $\mathbf{v}_h \in \mathbb{V}_0$, $q_h \in \mathbb{Q}_1$, then Σ_h^n is given by

$$D_{(\mathbf{u}_h^n, \Delta t)}^h \Sigma_h^n(\mathbf{x}_i) + \frac{1}{\text{Wi}} (\Sigma_h^n(\mathbf{x}_i) - \mathbf{I}) = 0. \quad (22)$$

At each mesh point, (22) is a coupled system of ordinary differential equations forced by the discrete fluid velocity via the deformation gradient, and approximated in an explicit manner, and therefore the nodal values may be updated without the need to solve a linear system.

Remark 5.5 (Choice of spatial discretisation points for finite difference scheme). *We note that since all derivatives appearing in the constitutive relation are approximated via (10), we are free to choose any set of points at which to approximate the conformation tensor, with the proviso that care must be taken to adequately resolve the velocity gradient, as this is what forces the constitutive law. The choice of these points so that they correspond with the degrees of freedom of a piecewise bilinear finite element space is a natural one, as it is then clear how to include the discrete conformation tensor in the momentum equation. Other possible choices are discussed in §7.*

Proposition 5.6. *If the initial condition σ^0 is positive definite, and bilinear interpolation is used to obtain Σ_h^0 and to evaluate Σ_h^k at points which are not vertices of the mesh, then at each time step there exists $\Delta t > 0$ such that the discrete conformation tensor remains positive definite.*

Proof. By assumption, all nodal values of Σ_h^{n-1} are positive definite. Then since interpolated values are weighted sums of the nodal values with non-negative weights, the interpolant is also positive definite. By the same argument as in Proposition 4.10, if we choose $\Delta t \leq \frac{1}{2} \|\mathbf{u}_h^n\|_{1,\infty}$, and if Σ_h^{n-1} is positive definite, then Σ_h^n computed from the scheme (22) will also be positive definite. \square

6 Numerical Experiments

In this section, we present numerical results obtained by solving (21)-(22) for a variety of model and discretisation parameters. All simulations presented here were conducted using `deal.II`, an open source C++ software library providing tools for finite element computations [2].

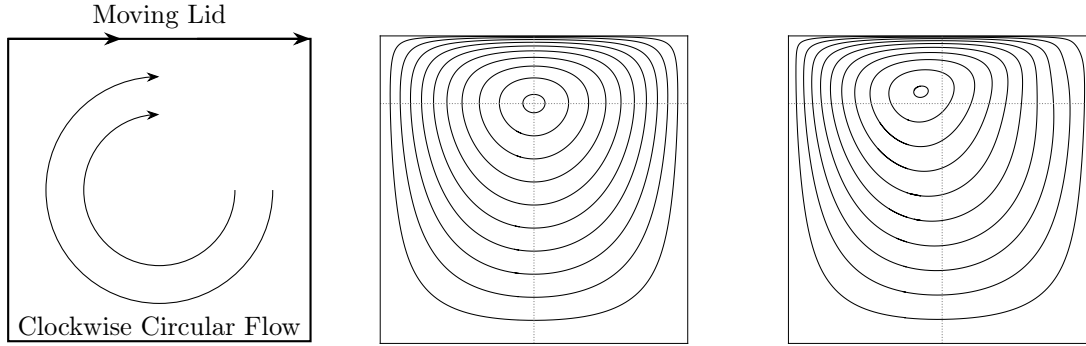


Figure 2: An illustration of a lid driven cavity setup (left). Streamlines of a Newtonian Stokes flow (middle) with left-right symmetry in the velocity magnitude. Introducing a polymeric stress breaks this symmetry, with the centre of circulation moving up and to the left with increasing Wi (right).

6.1 Description of the test case

The lid-driven cavity consists of a fluid-filled, impenetrable box in which the flow is driven by a moving lid. The flow of a Newtonian fluid in a lid-driven cavity is by now a very well studied problem. It is known that the flow characteristics, see Figure 2, depend upon the Reynolds number. Studies from the numerical literature largely agree with one another qualitatively and quantitatively for moderate Reynolds numbers. For larger Reynolds numbers, numerical solutions become more challenging, and differences appear in computational results. Detailed numerical studies have provided benchmarks for Reynolds numbers in the tens of thousands [9, 17].

In experimental studies, for small Reynolds number, flow in the cavity reaches a steady state, and, in a three dimensional cavity, remains approximately two dimensional. For the setup in Figure 2, i.e., with lid moving left to right, as the Reynolds number increases the centre of the main vortex moves to the right. Above a critical value of the Reynolds number, the flow transitions to a time-periodic state with variation in the neutral direction [1]. Even for inertialess non-Newtonian flows, the symmetry of the flow is broken (see Figure 2, right) and moves towards the upper left corner with increasing Weissenberg number [33].

In this work, the regularised lid-driven cavity problem was solved, for which $\Omega = [0, 1] \times [0, 1]$, $\mathbf{u} = (0, 0)^T$ on the lateral and lower boundaries, and on the lid (i.e. $\{(x_1, x_2) : x_2 = 1\}$), the velocity boundary condition is

$$\mathbf{u}_{lid}(\mathbf{x}, t) = 8 \left(1 + \tanh \left(8 \left(t - \frac{1}{2} \right) \right) \right) x_1^2 (1 - x_1^2), 0)^T.$$

Remark 6.1. For this problem, a Weissenberg number can be defined as

$$Wi = \frac{\lambda U}{H},$$

where λ is a characteristic relaxation time of the fluid, U is a characteristic velocity scale and H is the height of the cavity. Thus, U/H is a measure of the shear rate [33]. For the setup described above, $U = 1$, $H = 1$.

Table 1: Mesh statistics

Mesh	# elements	h_{\min}	h_{\max}
\mathcal{T}_{90}	8,100	0.0039	0.024
\mathcal{T}_{120}	14,400	0.0020	0.022
\mathcal{T}_{150}	22,500	0.0010	0.021
\mathcal{T}_{180}	32,400	0.00054	0.021
\mathcal{R}_{256}	65,536	1.5×10^{-5}	7.8×10^{-3}

6.2 Mesh design

Mesh design and selection of discretisation parameters appears to be of crucial importance for the cavity flow of an Oldroyd-B fluid, and indeed very few studies have reported satisfactory numerical results for the lid-driven cavity using a uniform mesh, with the notable exception of schemes which utilise the log-conformation tensor formulation. In addition, results for some schemes have been shown to be very sensitive to mesh size, for example in [7], dissipation properties, positive definiteness of the conformation tensor and existence of steady state change qualitatively upon varying the mesh size.

For the cavity problem, graded meshes of various types are a common choice. Meshes constructed in this manner are able to provide very fine resolution near the boundary (particularly the lid), where it is most needed, in an efficient manner. The situation may be compared to singularly perturbed convection-diffusion problems, which exhibit boundary layers that put severe limitations on the mesh size. To make computations tractable, layer-adapted meshes have been extensively researched in this community (see [27] for a review). A particularly effective example is the Bakhvalov-type mesh, where upper bounds on the derivatives of the solution near the boundary are used to design mesh grading functions that are sufficient to resolve it.

In this work, we will use a mixture of the following. One construction consists of decreasing element size towards the boundary with a constant contraction ratio γ , i.e. $h_{i+1} = \gamma h_i$ where the index i is such that $i + 1$ is the next element in the direction of the boundary [10, 43]. Another is to decrease element size by a constant amount c so that $h_{i+1} = h_i - c$ [34]. For comparison, the latter is equivalent to decreasing the contraction ratio, so that elements size decreases very rapidly near the boundary. Finally, in [19], mixtures of uniform grid spacing and refined areas are used.

Meshes constructed from central square elements with a constant reduction ratio of 0.96 towards each boundary are denoted by \mathcal{T}_N , where N is the number of elements in each coordinate direction. We denote by \mathcal{R}_N meshes constructed with linearly decreasing element size as follows (similar to those used in [34]). We define vertices for an $N \times N$ quadrilateral mesh by their x and y coordinates, given respectively by $x_i = 2 \left(\frac{i}{N}\right)^2$ for $i = 0, 1, \dots, \frac{N}{2}$, with $x_i = 1 - x_{N-i}$ for $i = \frac{N}{2} + 1, \dots, N$, and $y_i = 1 - \left(1 - \frac{i}{N}\right)^2$ for $i = 0, \dots, N$. On these meshes, the finest vertical resolution occurs at the lid, with an element height of $\frac{1}{N^2}$.

This means the meshes are highly anisotropic away from the corners. Stabilised finite element methods often have stabilisation parameters that depend badly on the anisotropy of the elements, however the solver we used (16) is parameter free.

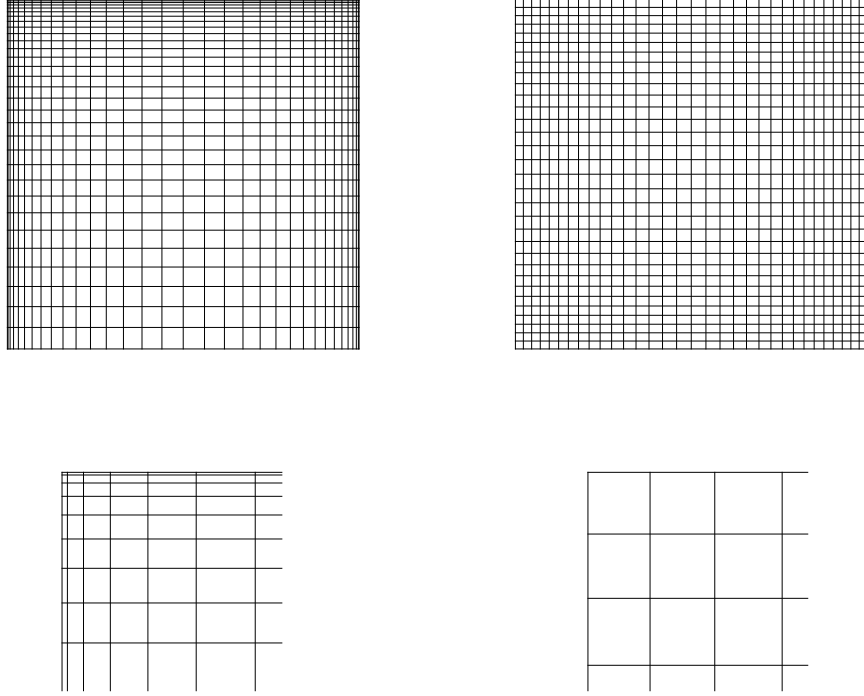


Figure 3: Illustrations of the two types of graded mesh used. Both meshes consist of 1024 elements. Left: mesh \mathcal{R}_{32} , offering aggressive refinement near the boundary. Right: \mathcal{T}_{32} . Bottom row: zoom of upper left corners showing an area of 0.08×0.08 to illustrate the differences in grading.

Table 2: Comparison of results with published data for the (regularised) lid-driven cavity, $\beta = 0.5$. Value marked * was estimated from [34] using their predicted relationship between this quantity and Wi (see [34, §4.3]), while values marked \dagger were estimated using a plot digitisation tool [38]. All other values were reported directly. All values from the current work were taken after a steady state had been reached (approx $t = 10$ for $Wi = 0.5$ and $t = 30$ for $Wi = 1$).

Reference	$\max_{x=0.5} \ln(\sigma_{11})$	$\max \sigma_{11}$	x_c, y_c
$Wi = 0.5$			
Current work \mathcal{T}_{90}	5.76	351.21	0.466, 0.799
Current work \mathcal{T}_{120}	5.65	309.65	0.466, 0.799
Current work \mathcal{T}_{150}	5.60	295.04	0.467, 0.799
Current work \mathcal{R}_{256}	5.59	290.59	0.467, 0.799
Pan et al. [34]	5.59 †	289*	0.469, 0.798
Sousa et al. [43] M4	5.51	-	0.466, 0.800
$Wi = 1$			
Current work \mathcal{T}_{180}	10.75	48,038.9	0.428, 0.819
Current work \mathcal{R}_{256}	10.22	28,069.2	0.431, 0.819
Pan et al. [34]	9.35 †	11,529.43	0.439, 0.816
Sousa et al. [43] M4	7.80	-	0.434, 0.816

6.3 Numerical results

Where possible, the results presented here are compared with the literature, particularly [16, 34, 43] - see Table 2. Descriptions of the meshes used are given in §6.2, and a summary of the key statistics of each is given in Table 1. The data for comparison are the logarithm of the maximum value of σ_{11} along the midline, $x = 0.5$, the maximum value of σ_{11} over the domain, and the coordinates of the centre of the main vortex, x_c, y_c .

6.3.1 $Wi = 0.5$

The solution appears to have reached a steady state by $t = 8$. In Figure 4, components of the conformation tensor are plotted along cross sections of the domain for $Wi = 0.5$ and for various computational meshes described in §6.2 and Table 1. The solutions obtained for σ_{11} and σ_{22} agree qualitatively very well with Figure 5 of [34], albeit with differences in magnitude along the lid. We note that the meshes used there are finer, which could account for the difference. Other metrics available for comparison from the numerical literature (see Table 4 in [43] and Table 2) are the centre of the main vortex in the velocity field and the logarithm of the maximum value of σ_{11} attained along the line $x = 0.5$. Computed on mesh \mathcal{R}_{256} , the former agrees very closely (within 1%) although not much variation in prediction of this quantity is observed across the numerical literature. The latter is approximately 2% larger than the other predictions given in [43]. Resolution of the layer at the top boundary appears to be of critical importance for the accuracy of the approximation. Under-resolution results in altered behaviour of σ_{12} at the upper boundary. In addition, coarse meshes appear to over-estimate σ_{11} . These errors do not appear to pollute the solution away from the boundary.

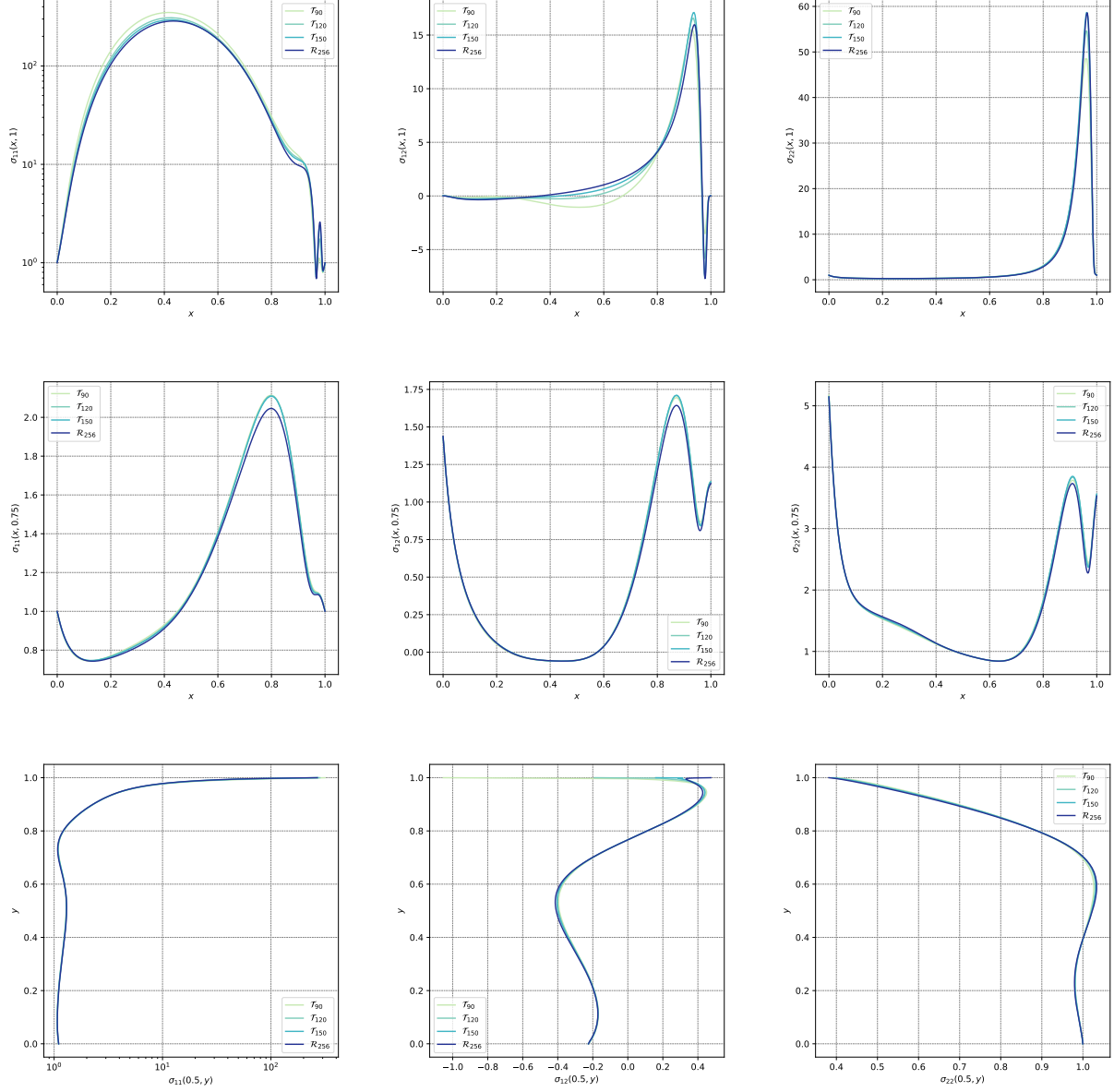


Figure 4: Components of the conformation tensor plotted along cross sections of the domain, obtained on meshes \mathcal{T}_{90} , \mathcal{T}_{120} , \mathcal{T}_{150} and \mathcal{R}_{256} with $Wi = 0.5$ and $t = 10$. Top row: plots over the top boundary given by $y = 1$. Middle row: plots over the line given by $y = 0.75$. Bottom row: plots over the midline given by $x = 0.5$.

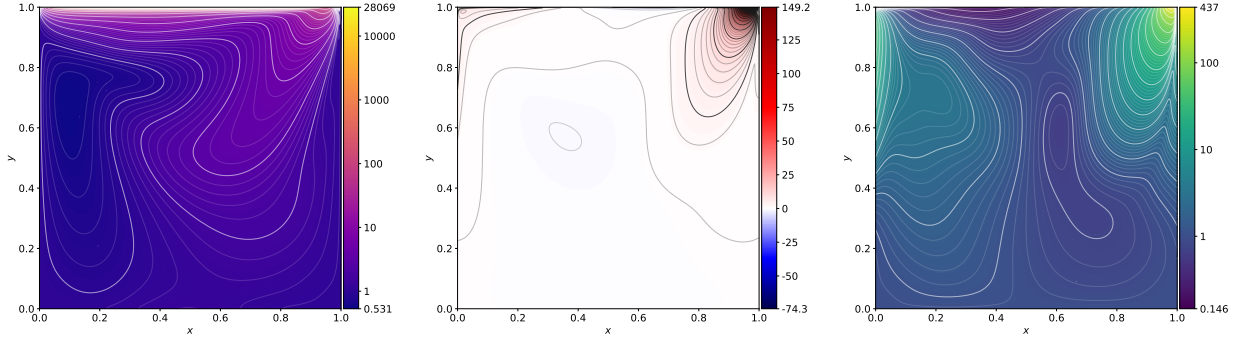


Figure 5: $Wi = 1$. Components of the conformation tensor at $t = 30$: σ_{11} , σ_{12} , σ_{22} (note σ_{11} and σ_{22} are logarithmically coloured and contoured while σ_{12} is linearly coloured and contoured). Different colormaps are used to emphasise the difference in magnitude between the components. Minimum and maximum values are shown on the colour bar.

6.3.2 $Wi = 1$

The solution appears to have reached a steady state by $t = 27.5$. The conformation tensor field is plotted component-wise in Figure 5, with benchmark metrics reported in Table 2. The logarithm of the conformation tensor was computed to allow comparison with other published works, with selected cross sections presented in Figure 6. A sharp boundary layer at the lid is observed in σ_{11} , with all components exhibiting large gradients near the upper corners of the domain. Our computational results agree qualitatively with those presented in [16, Figure 4], although in our simulations a steady state was reached much later than $t = 8$, as reported there. In addition, the maximum value σ_{11} along $x = 0.5$ was significantly overestimated in our work relative to other published data, but there is significant variation in this figure, with [34] reporting a value two logarithmic orders larger than [16]. However, it can be seen from Figure 6 that large discrepancies occur only in a very small neighbourhood of the upper boundary. Qualitative differences are observed only in the upper right hand corner.

In Figure 7, components of the conformation tensor are plotted along cross sections for two Weissenberg numbers, 0.5 and 1, to illustrate the difference in solutions. Larger magnitudes and exaggerated features are observed in all components for $Wi = 1$ when compared with $Wi = 0.5$.

6.4 Positive definiteness of the discrete conformation tensor

A major aim of the numerical scheme presented is to maintain a positive definite conformation tensor, both to respect the physics of the problem and avoid numerical instabilities that can arise when this property is lost. We recall from Proposition 5.6 that this is guaranteed if the time step is chosen to be sufficiently small. To ensure that an appropriate choice was made, the eigenvalues of the discrete conformation tensor were computed, and indeed at all times, the smallest eigenvalue of the conformation tensor was strictly positive, and therefore the discrete conformation tensor remained positive definite throughout the computation. The eigenvalues of the conformation tensor are visualised in Figure 8.

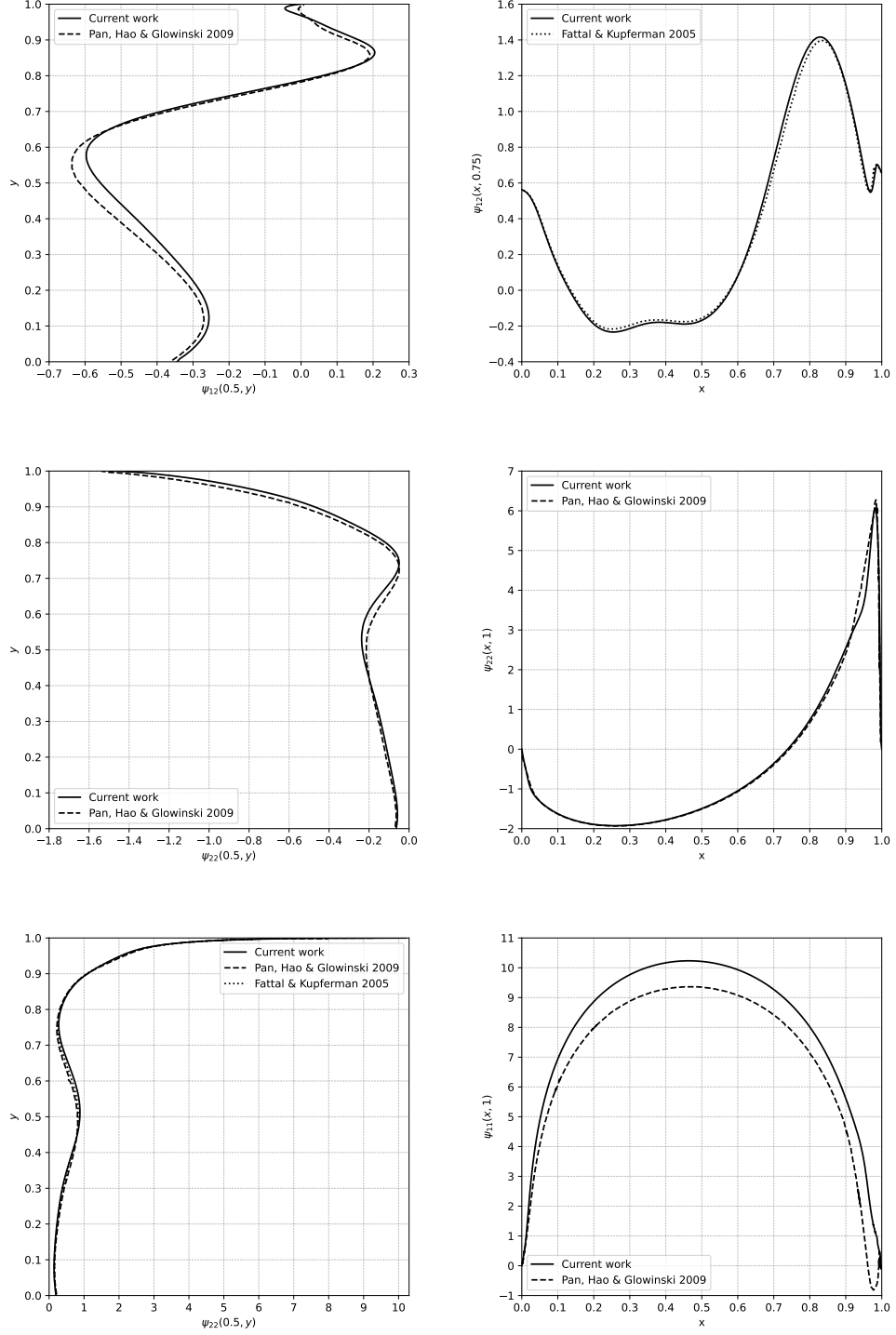


Figure 6: Components of the logarithm of the conformation tensor plotted along cross sections of the domain obtained on the mesh \mathcal{R}_{256} with $Wi = 1$ (solid line). Dotted line is numerical data from Fattal & Kupferman (2005) [16], while the dashed line is data from Pan, Hao & Glowinski (2009) [34].

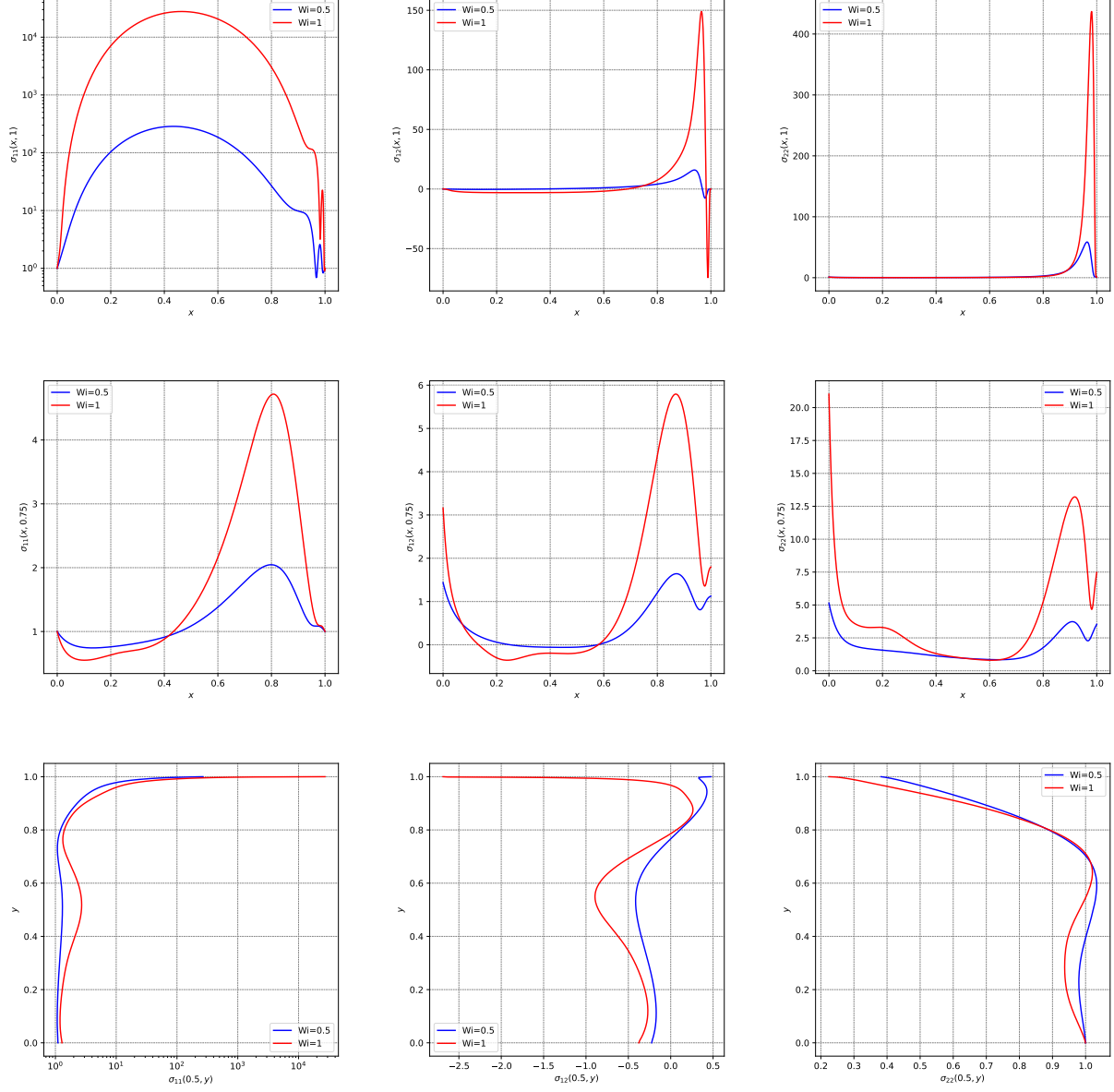


Figure 7: Components of the conformation tensor plotted along cross sections of the domain obtained on the mesh \mathcal{R}_{256} with $Wi = 0.5, 1$. Top row: plots over the top boundary given by $y = 1$. Middle row: plots over the line given by $y = 0.75$. Bottom row: plots over the midline given by $x = 0.5$.

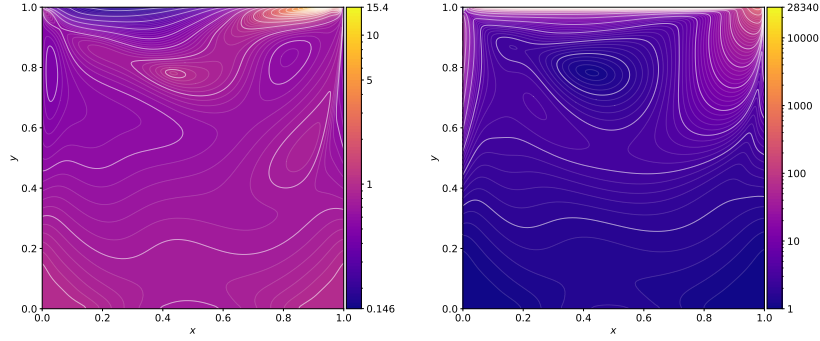


Figure 8: Left: Smallest eigenvalue of the discrete conformation tensor. Right: largest eigenvalue. Both plots are logarithmically coloured and contoured. Minimum and maximum values are shown on the colour bar.

7 Conclusions & Discussion

Results from simulations of an Oldroyd-B fluid in the creeping flow regime using a discretisation of the Lie derivative (7) were presented. The scheme maintained positive definiteness of the discrete conformation tensor and achieved good agreement with existing published data. Our proposed finite difference method circumvents quadrature issues, representing advection effectively compared to some finite element schemes, which can under-represent advection for small time steps or coarse quadrature formulas [8].

Qualitatively and quantitatively, the results are consistent with those in the literature using the log-conformation representation [16, 34, 43]. The scheme’s update process for the conformation tensor is efficient and straightforward to implement. However, spatial resolution and mesh design significantly influence the results, requiring fine meshes for convergence.

Further work includes exploring enhancements to preserve additional fluid structures, particularly incompressibility constraints and investigating differential equations on the special linear group for a consistent discrete deformation gradient. This may involve combining the approach with divergence-free finite element methods for fluid equations or exploring finer meshes or different finite difference points for the constitutive law to address challenges in the creeping flow regime.

8 Acknowledgements

This work has been partially supported by the Leverhulme Trust Research Project Grant No. RPG-2021-238. TP is also partially supported by EPSRC grants [EP/W026899/2](#), [EP/X017206/1](#) and [EP/X030067/1](#). The authors also want to thank Gabriel Barrenechea and Emmanuil Geourgoulis for helpful discussions and suggestions.

References

- [1] C. K. Aidun, N. Triantafilopoulos, and J. Benson. “Global stability of a lid-driven cavity with through-flow: Flow visualization studies”. In: *Physics of Fluids A: Fluid Dynamics* 3.9 (1991), pp. 2081–2091.
- [2] D. Arndt et al. “The deal.II finite element library: Design, features, and insights”. In: *Computers & Mathematics with Applications* 81 (2021), pp. 407–422. ISSN: 0898-1221. DOI: [10.1016/j.camwa.2020.02.022](https://doi.org/10.1016/j.camwa.2020.02.022). URL: <https://arxiv.org/abs/1910.13247>.
- [3] M. Bensaada, D. Esselaoui, and P. Saramito. “Error estimate for the characteristic method involving Oldroyd derivative in a tensorial transport problem”. In: *Electronic Journal of Differential Equations* (2004).
- [4] R. B. Bird, R. C. Armstrong, and O. Hassager. *Dynamics of polymeric liquids. Vol. 1: Fluid mechanics*. John Wiley and Sons Inc., New York, NY, 1987.
- [5] P. B. Bochev, C. R. Dohrmann, and M. D. Gunzburger. “Stabilization of low-order mixed finite elements for the Stokes equations”. In: *SIAM Journal on Numerical Analysis* 44.1 (2006), pp. 82–101.
- [6] J. Bonvin, M. Picasso, and R. Stenberg. “GLS and EVSS methods for a three-field Stokes problem arising from viscoelastic flows”. In: *Computer Methods in Applied Mechanics and Engineering* 190.29-30 (2001), pp. 3893–3914.
- [7] S. Boyaval. “Lid-driven-cavity simulations of Oldroyd-B models using free-energy-dissipative schemes”. In: *Numerical Mathematics and Advanced Applications 2009: Proceedings of ENUMATH 2009, the 8th European Conference on Numerical Mathematics and Advanced Applications, Uppsala, July 2009*. Springer. 2010, pp. 191–198.
- [8] S. Boyaval, T. Lelièvre, and C. Mangoubi. “Free-energy-dissipative schemes for the Oldroyd-B model”. In: *ESAIM: Mathematical Modelling and Numerical Analysis* 43.3 (2009), pp. 523–561.
- [9] C.-H. Bruneau and M. Saad. “The 2D lid-driven cavity problem revisited”. In: *Computers & fluids* 35.3 (2006), pp. 326–348.
- [10] R. Comminal, J. Spangenberg, and J. H. Hattel. “Robust simulations of viscoelastic flows at high Weissenberg numbers with the streamfunction/log-conformation formulation”. In: *Journal of Non-Newtonian Fluid Mechanics* 223 (2015), pp. 37–61.
- [11] J. Dealy. “Weissenberg and Deborah numbers—their definition and use”. In: *Rheol. Bull* 79.2 (2010), pp. 14–18.
- [12] C. R. Dohrmann and P. B. Bochev. “A stabilized finite element method for the Stokes problem based on polynomial pressure projections”. In: *International Journal for Numerical Methods in Fluids* 46.2 (2004), pp. 183–201.
- [13] F. Dupret and J. Marchal. “Sur le signe des valeurs propres du tenseur des extra-contraintes dans un écoulement de fluide de Maxwell”. In: *Journal de mécanique théorique et appliquée* 5.3 (1986), pp. 403–427.
- [14] H. C. Elman, D. J. Silvester, and A. J. Wathen. *Finite elements and fast iterative solvers: with applications in incompressible fluid dynamics*. Oxford university press, 2014.

- [15] R. Fattal and R. Kupferman. “Constitutive laws for the matrix-logarithm of the conformation tensor”. In: *Journal of Non-Newtonian Fluid Mechanics* 123.2-3 (2004), pp. 281–285.
- [16] R. Fattal and R. Kupferman. “Time-dependent simulation of viscoelastic flows at high Weissenberg number using the log-conformation representation”. In: *Journal of Non-Newtonian Fluid Mechanics* 126.1 (2005), pp. 23–37.
- [17] U. Ghia, K. N. Ghia, and C. Shin. “High-Re solutions for incompressible flow using the Navier-Stokes equations and a multigrid method”. In: *Journal of computational physics* 48.3 (1982), pp. 387–411.
- [18] G. H. Golub and C. F. Van Loan. *Matrix computations*. JHU press, 2013.
- [19] F. Habla, M. W. Tan, J. Haßlberger, and O. Hinrichsen. “Numerical simulation of the viscoelastic flow in a three-dimensional lid-driven cavity using the log-conformation reformulation in OpenFOAM®”. In: *Journal of Non-Newtonian Fluid Mechanics* 212 (2014), pp. 47–62.
- [20] E. Hairer, M. Hochbruck, A. Iserles, and C. Lubich. “Geometric numerical integration”. In: *Oberwolfach Reports* 3.1 (2006), pp. 805–882.
- [21] J. Hinch and O. Harlen. “Oldroyd B, and not A?” In: *Journal of Non-Newtonian Fluid Mechanics* 298 (2021), p. 104668.
- [22] T. J. Hughes. “Numerical implementation of constitutive models: rate-independent deviatoric plasticity”. In: *Theoretical foundation for large-scale computations for nonlinear material behavior: Proceedings of the Workshop on the Theoretical Foundation for Large-Scale Computations of Nonlinear Material Behavior Evanston, Illinois, October 24, 25, and 26, 1983*. Springer. 1984, pp. 29–63.
- [23] M. A. Hulsen, R. Fattal, and R. Kupferman. “Flow of viscoelastic fluids past a cylinder at high Weissenberg number: stabilized simulations using matrix logarithms”. In: *Journal of Non-Newtonian Fluid Mechanics* 127.1 (2005), pp. 27–39.
- [24] A. Jafari, A. Chitsaz, R. Nouri, and T. N. Phillips. “Property preserving reformulation of constitutive laws for the conformation tensor”. In: *Theoretical and Computational Fluid Dynamics* 32 (2018), pp. 789–803.
- [25] Y.-J. Lee and J. Xu. “New formulations, positivity preserving discretizations and stability analysis for non-Newtonian flow models”. In: *Computer methods in applied mechanics and engineering* 195.9-12 (2006), pp. 1180–1206.
- [26] Y.-J. Lee, J. Xu, and C.-S. Zhang. “Stable finite element discretizations for viscoelastic flow models”. In: *Handbook of numerical analysis*. Vol. 16. Elsevier, 2011, pp. 371–432.
- [27] T. Linß. “Layer-adapted meshes for convection–diffusion problems”. In: *Computer Methods in Applied Mechanics and Engineering* 192.9-10 (2003), pp. 1061–1105.
- [28] A. Lozinski and R. G. Owens. “An energy estimate for the Oldroyd B model: theory and applications”. In: *Journal of non-newtonian fluid mechanics* 112.2-3 (2003), pp. 161–176.
- [29] M. Lukáčová-Medvid’ová, H. Notsu, and B. She. “Energy dissipative characteristic schemes for the diffusive Oldroyd-B viscoelastic fluid”. In: *International Journal for Numerical Methods in Fluids* 81.9 (2016), pp. 523–557.

- [30] D. D. Medeiros, H. Notsu, and C. M. Oishi. “Second-order finite difference approximations of the upper-convected time derivative”. In: *SIAM Journal on Numerical Analysis* 59.6 (2021), pp. 2955–2988.
- [31] J. G. Oldroyd. “On the formulation of rheological equations of state”. In: *Proceedings of the Royal Society of London. Series A. Mathematical and Physical Sciences* 200.1063 (1950), pp. 523–541.
- [32] P. Pakdel and G. H. McKinley. “Cavity flows of elastic liquids: purely elastic instabilities”. In: *Physics of Fluids* 10.5 (1998), pp. 1058–1070.
- [33] P. Pakdel, S. H. Spiegelberg, and G. H. McKinley. “Cavity flows of elastic liquids: two-dimensional flows”. In: *Physics of Fluids* 9.11 (1997), pp. 3123–3140.
- [34] T.-W. Pan, J. Hao, and R. Glowinski. “On the simulation of a time-dependent cavity flow of an Oldroyd-B fluid”. In: *International Journal for Numerical Methods in Fluids* 60.7 (2009), pp. 791–808.
- [35] J. Petera. “A new finite element scheme using the Lagrangian framework for simulation of viscoelastic fluid flows”. In: *Journal of non-newtonian fluid mechanics* 103.1 (2002), pp. 1–43.
- [36] F. Pimenta and M. Alves. “Stabilization of an open-source finite-volume solver for viscoelastic fluid flows”. In: *Journal of Non-Newtonian Fluid Mechanics* 239 (2017), pp. 85–104.
- [37] O. Pironneau. “On the transport-diffusion algorithm and its applications to the Navier-Stokes equations”. In: *Numerische Mathematik* 38 (1982), pp. 309–332.
- [38] *PlotDigitizer: Version 3.1.5*. 2023. URL: <https://plotdigitizer.com>.
- [39] M. Renardy. *Mathematical analysis of viscoelastic flows*. SIAM, 2000.
- [40] M. Renardy and B. Thomases. “A mathematician’s perspective on the Oldroyd B model: Progress and future challenges”. In: *Journal of Non-Newtonian Fluid Mechanics* 293 (2021), p. 104573.
- [41] H. Rui and M. Tabata. “A second order characteristic finite element scheme for convection-diffusion problems”. In: *Numerische Mathematik* 92.1 (2002), pp. 161–177.
- [42] I. Rutkevich. “The propagation of small perturbations in a viscoelastic fluid”. In: *Journal of Applied Mathematics and Mechanics* 34.1 (1970), pp. 35–50.
- [43] R. Sousa, R. Poole, A. Afonso, F. Pinho, P. Oliveira, A. Morozov, and M. Alves. “Lid-driven cavity flow of viscoelastic liquids”. In: *Journal of Non-Newtonian Fluid Mechanics* 234 (2016), pp. 129–138.
- [44] E. Süli. “Convergence and nonlinear stability of the Lagrange-Galerkin method for the Navier-Stokes equations”. In: *Numerische Mathematik* 53 (1988), pp. 459–483.
- [45] W.-H. Zhang, J. Li, Q. Wang, Y. Ma, H.-N. Zhang, B. Yu, and F. Li. “Comparative study on numerical performances of log-conformation representation and standard conformation representation in the simulation of viscoelastic fluid turbulent drag-reducing channel flow”. In: *Physics of Fluids* 33.2 (2021).